Modelling and performance evaluation of a low-temperature ammonia–water absorption refrigeration system

Y.T. Ge[1,*], S.A. Tassou[1] and I. Chaer[2]

[1]*Mechanical Engineering, School of Engineering and Design, Brunel University, Uxbridge, Middlesex UB8 3PH, UK*

[2]*Faculty of Engineering, Science and the Built Environment, London South Bank University (T617), Borough Road, London SE1 0AA, UK*

Abstract

This paper presents the simulation of a low-temperature gas-fired ammonia–water absorption chiller for refrigeration applications. The model was developed as part of a research effort to investigate microturbine-based tri-generation systems for application in the food retail industry. The absorption chiller model was developed in the TRNSYS environment by integrating the main component models in the system and will form part of an overall TRNSYS-based supermarket model. The chiller model was validated against experimental results obtained on a 12 kW absorption chiller in the laboratory. The model was subsequently used to investigate the influence of important design and operating parameters on the performance of the chiller.

Keywords: ammonia–water absorption chiller; modelling and validation; low-temperature refrigeration

*Corresponding author:
yunting.ge@brunel.ac.uk

Received 6 May 2009; revised 11 May 2009; accepted 12 May 2009

1 INTRODUCTION

Gas-fired absorption chillers can offer advantages over electrically driven machines in applications where the local electrical supply grid has insufficient capacity and where noise is a consideration. Other advantages of absorption chillers include the use of environmental-friendly refrigerants and the possibility to use waste heat or the exhaust gases of local combined heat and power systems to drive the generator. Most applications of absorption chillers have been in the air-conditioning field where the flow temperature required is above 6°C. These chillers invariably use lithium bromide–water as fluid pair with water being the refrigerant and lithium bromide the absorbent. There have also been applications of absorption chillers at temperatures down to −55°C or even lower in the chemical and food manufacturing industries, but these have been of the specially made type using ammonia–water as fluid pair with ammonia being the refrigerant and water the absorbent [1,2]. More recently, small packaged ammonia–water chillers have become available in the market and this has prompted their evaluation for a wide range of applications at temperatures below 0°C. An example of this is the Robur unit which provides a refrigeration capacity of 12 kW at −12°C flow temperature. A schematic diagram of this chiller is shown in Figure 1. A similar type of chiller was modelled by Lazzarin *et al.* [3,4] with the integration of the main component models in the system. Of the component models, the generator was divided into two control volumes while other components had one control volume each. The system model was validated by comparing the cooling capacities from manufacture at conditions of different temperatures of air inlet and brine outlet. The model was then utilized to predict the variations of solution concentrations, high and low solution pressures, component heat fluxes and cooling capacities with the temperatures of air inlet and brine outlet. Some constant parameters were assumed for the component models such as the effectiveness for generator, condenser and evaporator, the temperature differences between solution and air for the air-cooled heat exchanger, and the temperature differences between vapour and solution for the rectifier. These constant parameters which are critical to the model accuracy can be determined by further experiments of the chiller at different conditions.

Experimental investigations on the similar type of chiller with different chilled solution and various structure of

International Journal of Low-Carbon Technologies 2009, 4, 68–77

doi:10.1093/ijlct/ctp015 Advance Access Publication 4 June 2009

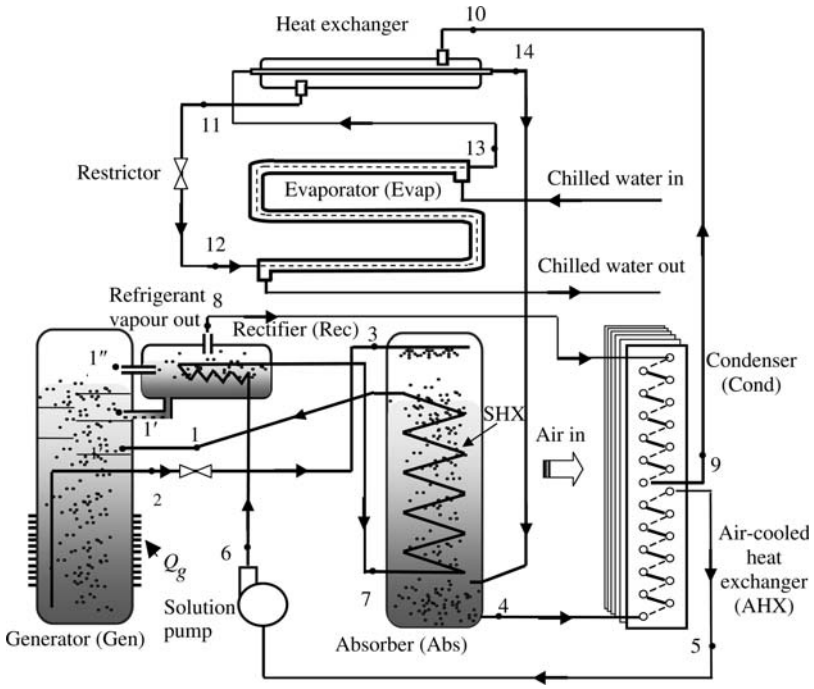

Figure 1. *Schematic diagram of the absorption refrigeration system.*

evaporator were carried out by Horuz *et al.* [5]. Water-cooled absorber and condenser were introduced in addition to the original air-cooled ones so as to examine the system performance under the conditions of a wider range of high-side pressures. The experimental investigations were carried out under six different operating conditions including variable chilled water inlet temperature and flow rate, changeable chilled water level in the evaporator drum, varied generator heat input, and different cooling water flow rate and inlet temperature to the water-cooled condenser. It was found that the cooling capacity, component heat transfer rates, and cooling coefficient of performance (COP) were all increased with higher chilled water inlet temperature. In the mean time, the above three performance parameters were all increased with elevated energy input to generator. In addition, the cooling capacity and COP were both augmented with increased condenser cooling water flow rate but the COP was decreased with higher condenser cooling water temperature. The solution high and low pressures which were quite important to the system performance were however not presented.

The models of different types of absorption refrigeration systems were reported in series by Grossman *et al.* [6-10] and were finalized into a modular simulation tool—ABSIM for advanced absorption systems. The codes underneath the system models are based on unit subroutines containing the governing equations for the system's components. Each component is assumed as one control volume and the applied governing equations for the control volume are similar to those used by Lazzarin *et al.* [3,4]. Based on user-supplied cycle diagrams, working fluid and given operating conditions, the model calculates the properties at each state point in the system cycle and the thermal duty of each component. For the solution to converge, it requires careful selection of input parameters, such as the UA or effectiveness values of the heat transfer components. This makes the model difficult to use by inexperienced users. To obtain a reasonable prediction of system performance by the model, the correlated value of UA or effectiveness for each component from test results is still needed.

Apart from the above system models formed by the integration of simplified component models, the detailed component models are still significant to describe operationally and assist the optimal designs for the components. Chua *et al.* [11] developed a detailed absorption generator model in which the multi-stream non-isothermal heat and mass transfers were recognized and considered. Goel *et al.* [12] developed an analytical model to simulate the combined heat and mass transfer process in a counter-current ammonia–water-based absorber. The model requires detailed description of the geometric characteristics of the absorber. It uses empirical correlations to predict the heat and mass transfer coefficients and accounts for both liquid and vapour phase mass transfer resistances. Similar investigations on absorbers were carried out by Kaynakli *et al.* [13] and Kwon *et al.* [14]. All these models require detailed description of the components' geometric data, which inversely limits their applications to different types of system.

Any simulation model requires a method for calculating the thermophysical properties of the fluid pair in the system. A simple, practical and fairly accurate method to do this for the ammonia–water fluid pair was proposed by Conde [15].

This paper presents a model of a low-temperature air-cooled ammonia–water absorption chiller system. The system model is an integration of the main component sub-models. To avoid the need to have detailed data on the geometric characteristics of the components and ensure speed of solution, each component model was based on the lumped parameter methodology. To facilitate the modelling processes, the generator and rectifier are combined into one control volume while the absorber is divided into two control volumes. In the mean time, extensive experiments were carried out including the variation of high and low solution pressures with the temperatures of air inlet and brine outlet. The test results are used to validate the model and correct the heat transfer parameters needed in the component models. The following sections describe the modelling methodology adopted, validation against experimental measurements and model applications. This is a first stage in the development of an integrated model of a microturbine-based tri-generation system for low-temperature food refrigeration applications.

2 MODELLING SCHEME WITH THE LUMPED METHOD

A schematic diagram of the refrigeration system considered in this investigation is shown in Figure 1. Referring to the diagram, the system consists of eight main components: generator, rectifier, air-cooled condenser, sub-cooling heat exchanger, liquid-cooling evaporator, absorber (solution-cooled), air-cooled heat exchanger and solution pump. After flowing through the generator and rectifier, the nearly pure refrigerant at '8' enters the air-cooled condenser where it is condensed to liquid at '9'. The refrigerant then passes through the connection pipes and arrives at '10'. From there the refrigerant flows through a tube-in-tube heat exchanger where it exchanges heat with the refrigerant vapour leaving the evaporator and is further subcooled at '11'. The refrigerant then flows through a thermodynamic expansion valve at '12' before entering the evaporator coil where it evaporates while absorbing heat from a brine solution.

The refrigerant vapour exiting the evaporator at '13' then flows through the tube-in-tube heat exchanger where it is superheated to '14' before entering the absorber. The 'strong' solution from the generator enters the absorber at '3' where it is first cooled by a solution heat exchanger (SHX) before absorbing the refrigerant flowing from the evaporator. It should be noted that in this paper 'strong' solution refers to a solution that is rich in absorbent, whereas 'weak' solution refers to a solution that is weak in absorbent and rich in refrigerant. The 'weak' solution formed in the absorber then flows through the air-cooled heat exchanger where the heat generated by the absorption process is rejected to the ambient. The solution then exits the heat exchanger at '5' and is pumped through the rectifier and absorber to the generator at '1'. The weak solution is heated and distilled in the generator and as a result, a strong solution is formed at the bottom of the generator and high concentration ammonia refrigerant at the top. The strong solution then exits the generator at '2' and flows through an expansion device before entering the absorber where it is sprayed over the SHX. The refrigerant flows from the top of the generator to the rectifier where more water in the ammonia refrigerant condenses and returns back to the generator. The nearly pure refrigerant then exits the rectifier at '8' and flows to the condenser for the repetition of the cycle.

The model of each component was developed based on the energy, mass and species conservation equations. For simplicity, each component was assumed as a single or two control volumes. The models of the more complicated components in the system are described as below.

2.1 Rectifier

The rectifier was assumed to be a single control volume. The assumptions made in developing the model are:

(1) Pure saturated refrigerant vapour at rectifier exit (point 8 in Figure 1).
(2) Saturated vapour solution at top of generator (point $1''$).
(3) Saturated liquid solution from rectifier to generator (point $1'$).
(4) No heat loss in rectifier.

Conservation of mass for ammonia:

$$(1+R)\xi_{1''} = \xi_8 + R\xi_{1'} \tag{1}$$

Conservation of energy:

$$(1+R)h_{1''} = h_8 + Rh_{1'} + q_r \tag{2}$$

where

$$R = \dot{m}_{1'}/\dot{m}_8$$

2.2 Generator and rectifier

The generator and rectifier are combined into one control volume to facilitate the modelling. Assumptions for the generator are:

(1) Saturated liquid for weak solution outlet of generator at '2'.
(2) No heat loss in generator.

Conservation of mass for ammonia:

$$f\xi_1 = (f-1)\xi_2 + \xi_8 \tag{3}$$

Conservation of energy:

$$q_g = h_8 - h_2 + q_r + f(h_2 - h_1) \tag{4}$$

where, in Equations (3) and (4)

$$f = \frac{\dot{m}_1}{\dot{m}_8}$$

2.3 Solution-cooled absorber

To simplify the simulation, the solution-cooled absorber was divided into two control volumes, CV_1 and CV_2, as shown in Figure 2. The simulation assumes that the weak solution exiting the solution cooled absorber is saturated liquid.

For control volume CV_1:Conservation of mass for solution:

$$\dot{m}_3 = \dot{m}_{3a} \tag{5}$$

Conservation of mass for ammonia:

$$\dot{m}_3 \xi_3 = \dot{m}_{3a} \xi_{3a} \tag{6}$$

Conservation of energy:

$$\dot{Q}_a = \dot{m}_7 (h_1 - h_7) = \dot{m}_3 (h_3 - h_{3a}) \tag{7}$$

Heat transfer:

$$\dot{Q}_a = \text{UA} \times \text{LMTD} \tag{8}$$

where

$$\text{LMTD} = \frac{\Delta T_{a,\max} - \Delta T_{a,\min}}{\ln\left(\Delta T_{a,\max} / \Delta T_{a,\min}\right)}$$
$$\Delta T_{a,\max} = \max(T_3 - T_1,\ T_{3a} - T_7)$$
$$\Delta T_{a,\min} = \min(T_3 - T_1,\ T_{3a} - T_7)$$

For control volume CV_2:
Conservation of mass for ammonia:

$$\dot{m}_{3a} \xi_{3a} + \dot{m}_{14} = \dot{m}_4 \xi_4 \tag{9}$$

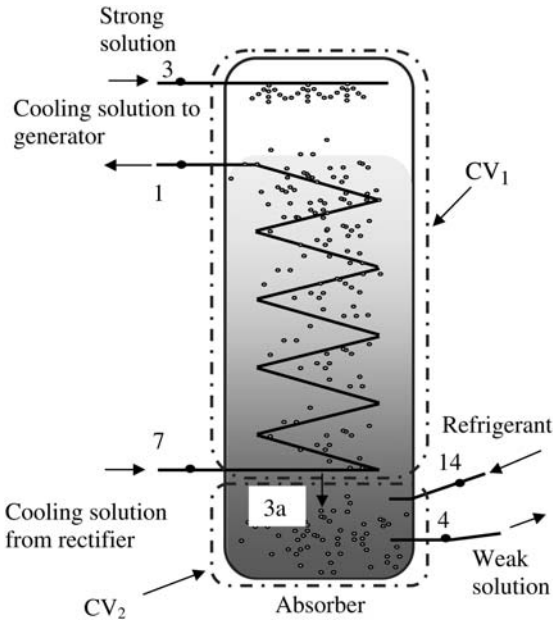

Figure 2. *Two control volumes of solution-cooled absorber.*

Conservation of energy:

$$\dot{m}_{3a} h_{3a} + \dot{m}_{14} h_{14} = \dot{m}_4 h_4 \tag{10}$$

2.4 Air-cooled heat exchanger

The conservation equations for the air-cooled heat exchanger are similar to those of equations in CV_1 of solution-cooled absorber except for the different endpoints of the two heat exchange sides. In this component model, the warm side is the weak solution and the cold side is air.

2.5 Air-cooled condenser

Conservation of energy:

$$\dot{Q}_c = \dot{m}_8 (h_8 - h_9) = \dot{m}_a C_{P_a} (T_{a_{out}} - T_{a_{in}}) \tag{11}$$

Heat transfer:

$$\dot{Q}_c = \text{UA} \times \text{LMTD} \tag{12}$$

where

$$\text{LMTD} = \frac{\Delta T_{c,\max} - \Delta T_{c,\min}}{\ln\left(\Delta T_{c,\max} / \Delta T_{c,\min}\right)}$$
$$\Delta T_{a,\max} = \max(T_8 - T_{a_{out}},\ T_9 - T_{a_{in}})$$
$$\Delta T_{a,\min} = \min(T_8 - T_{a_{out}},\ T_9 - T_{a_{in}})$$

2.6 Liquid-cooling evaporator

Conservation of energy:

$$\dot{Q}_e = \dot{m}_{12} (h_{13} - h_{12}) = \dot{m}_{cf} C_{P_{cf}} (T_{cf_{in}} - T_{cf_{out}}) \tag{13}$$

where

$$\dot{m}_{12} = \dot{m}_8$$

Heat transfer:

$$\dot{Q}_e = \text{UA} \times \text{LMTD} \tag{14}$$

where

$$\text{LMTD} = \frac{\Delta T_{e,\max} - \Delta T_{e,\min}}{\ln\left(\Delta T_{e,\max} / \Delta T_{e,\min}\right)}$$
$$\Delta T_{a,\max} = \max(T_{cf_{in}} - T_{13},\ T_{cf_{out}} - T_{12})$$
$$\Delta T_{a,\min} = \min(T_{cf_{in}} - T_{13},\ T_{cf_{out}} - T_{12})$$

As a result, system COP can be calculated as:

$$\text{COP} = \frac{Q_e}{Q_g + Q_p}$$

2.7 System model

The component models were integrated to form a system model within the TRNSYS [16] environment as shown in Figure 3. TRNSYS is a transient system simulation programme with a modular structure. It recognizes a system description language in which the user specifies the components that constitute the

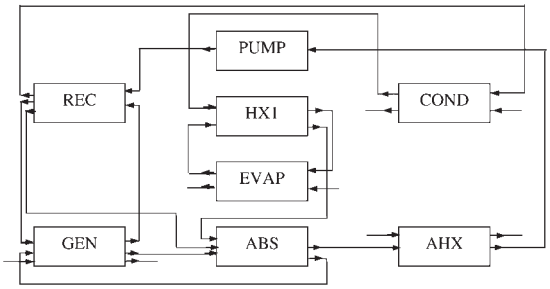

Figure 3. *Model of absorption chiller within the TRNSYS environment.*

system and the manner in which they are connected. The outputs of each component model can be inputs to another component according to the actual component layout in the system. The accuracy of the system simulation is dependent on the correctness of the component models and their integration.

Inputs to the system model include mass flow rate and temperature of chilled fluid at inlet to the evaporator and air at inlet to the condenser, heat input to generator, UA values for the heat exchange components and degrees of superheating and subcooling of the refrigerant at evaporator and condenser outlet, respectively. As a first step, assumptions are made for the pressures on both the high and low pressure sides of the system, and the mass flow rate and mass concentration of ammonia in the weak solution. Based on these initial assumptions, the equations for each component model on the high pressure side are solved through an iterative process around the degree of subcooling in the condenser as shown in Figure 4. Through each iteration the pressure in the high pressure side of the system is adjusted until the actual and desired values of subcooling agree to the required degree of accuracy. A similar procedure is then followed for the evaporator model where the pressure of the low pressure side of the system is adjusted until the actual and set value of superheat agree to the desired degree of accuracy. Once this is achieved, the model simulates the processes in the absorber and determines the concentration and enthalpy of the weak solution at the absorber outlet. If the enthalpy does not correspond to the saturation enthalpy at the absorber pressure, the concentration of the weak solution is adjusted until the weak solution at the absorber outlet is saturated liquid. Once this is achieved, the solution is further subcooled by the air-cooled heat exchanger. The pump model determines the input power, enthalpy and temperature of the weak solution entering the generator. If the concentration, temperature and mass flow rate of the weak solution entering the generator at point 1 are not close to the assumed or calculated values from the last iteration, then the model iterates on these values until convergence is achieved.

3 MODEL VALIDATION

The gas-fired ammonia–water absorption chiller, shown schematically in Figure 1, was used to obtain test results to validate the model. The chiller has a nominal refrigeration capacity of 12 kW at conditions of ambient air temperature of 35°C and chilled water flow temperature of −5°C.

The unit was installed and commissioned in the laboratory to facilitate the experimental investigations. The test facility is shown schematically in Figure 5. It consists of the air-cooled absorption chiller and an air-cooling loading circuit which is a cooling coil to heat up the low-temperature secondary refrigerant from the chiller and provide the refrigeration load to the chiller. The refrigeration load can be adjusted by modulating the fans' frequency to facilitate testing at a fluid temperature at the evaporator outlet down to −12°C. The fluid in the closed circuit was a mixture of 40% mass propylene glycol/water. The test facility was instrumented with pressure transducers of model OMGA PX771A-100DI with ±3 Pa accuracy to measure the pressures in the low and high pressure sides of the system; thermocouples with ±0.2°C accuracy to measure temperatures at various points in the refrigeration cycle, before and after each major component; thermocouples also with ±0.2 C accuracy to measure the temperature of the secondary fluid at inlet and outlet of the evaporator coil; a flow meter of model KROHNE IFC 010D with an accuracy 0.2% to measure the flow rate of the secondary fluid through the evaporator coil.

The experiments were carried out over a range of ambient temperatures between 16 ± 0.5°C and 17 ± 0.5°C and chilled water flow temperatures between −2°C and −12°C at a constant secondary fluid flow rate of 0.67 kg/s. Figure 6 shows the temperature test results for the ammonia–water solution at the inlets and outlets of generator and absorber. In the figure, T1, T2, T4 and T7 are referred to the solution temperatures at the generator inlet, generator outlet, absorber outlet and absorber cooler inlet, respectively.

Parameters used for model validation and component UA value adjustment are pressures in the low and high pressure sides of the system, cooling capacity and cooling COP. Figure 7 shows a comparison between the experimental and simulation results for the pressure in the high pressure (generator) side of the system for a range of ambient and chilled secondary fluid outlet temperatures. It can be seen that the pressure in the generator side of the system increases with increasing chilled fluid outlet temperature. Higher ambient temperatures also lead to slightly higher pressures on the high pressure side of the system. Simulation accuracy for the high pressure side is quite good.

Similar characteristics were obtained for the pressure in the low pressure side of the system. As can be seen from Figure 8, higher chilled fluid outlet temperatures lead to higher pressures. It can also be seen that ambient temperature has less effect on the low pressure side of the system. At low secondary fluid flow temperatures, below −5°C, the simulation accuracy is very good. At higher fluid flow temperatures, experimental and simulation results begin to diverge. This may be owing to the fixed UA values used in the simulation.

Figures 9 and 10 show the comparisons between the cooling capacity and cooling COP, respectively, determined from tests

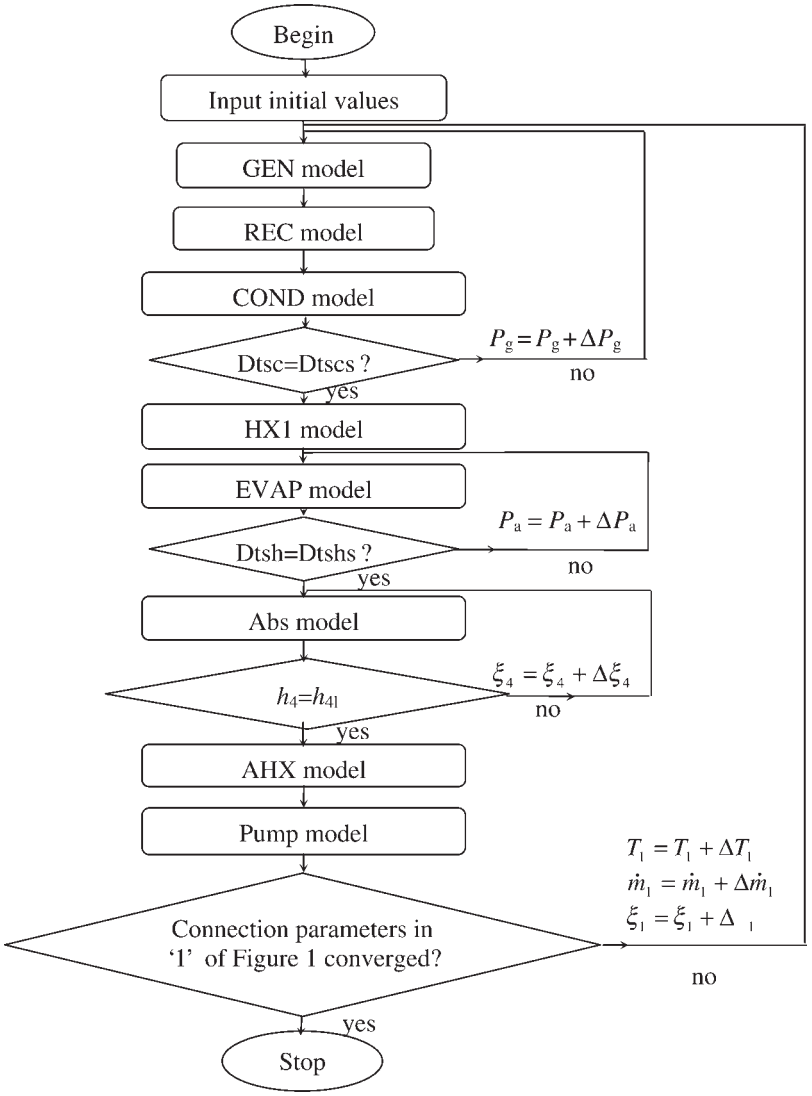

Figure 4. *Flowchart of system simulation.*

and simulation over a range of chilled fluid outlet temperatures and ambient temperatures. The scatters that can be observed in the experimental results are mainly because of the variation in ambient temperature during the tests and the slow response of the system to variations in both the ambient temperature and chilled fluid temperature. Despite the scatters, however, there are clear trends that show both cooling capacity and coling COP of the system to increase with increasing chilled fluid outlet tempertaure at specific ambient temperature. This is mainly because of the higher evaporating temperature, which leads to a higher refrigerant density and hence higher refrigerant flow rate in the system.

4 MODEL APPLICATION

The validated model can be used to explore the performance of the absorption unit at various operating conditions. In the experiments, the ambient temperature which is quite important to the system performance varied between 15.5°C and 17.5°C. To investigate the performance of the system over a wider range of ambient temperatures likely to be encountered in practice, simulations were carried out with ambient temperatures between 10°C and 30°C and chilled fluid flow temperatures between −30°C and 5°C.

Figure 11 shows the variation of ammonia concentration in the weak and strong solution with chilled fluid flow temperature and ambient temperature. It can be seen that both the strong and weak solution concentrations increase with chilled fluid temperature.

As the chilled fluid tmperature increases, the presures in both the low and high pressure sides of the system increase as shown in Figure 12. In addition, it shows that an increase in the ambient temperature leads to an increase in the pressure in the condenser and the generator but has little effect on the pressure in the evaporator and absorber.

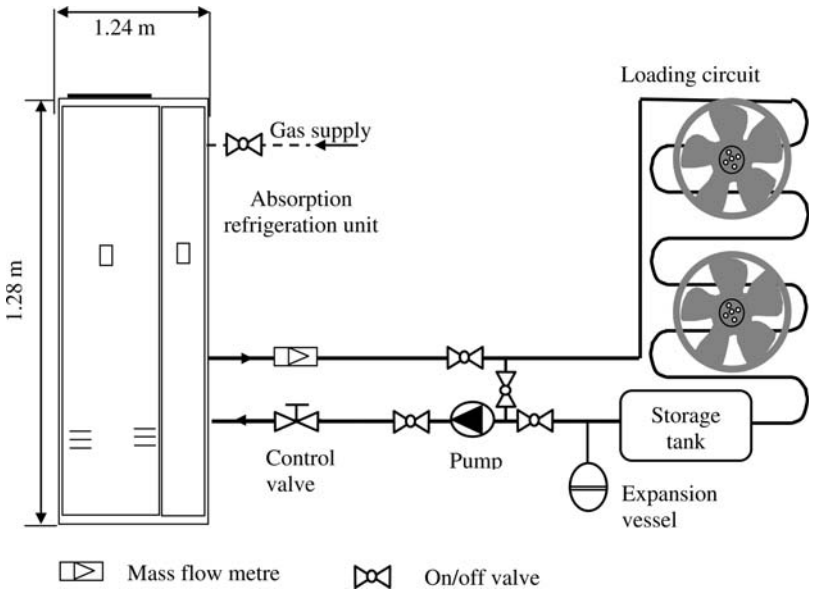

Figure 5. *Schematic diagram of the experimental facility.*

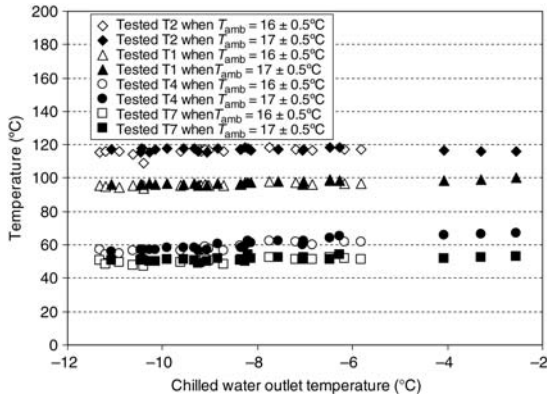

Figure 6. *Tested ammonia water solution temperatures at generator and absorber inlets and outlets.*

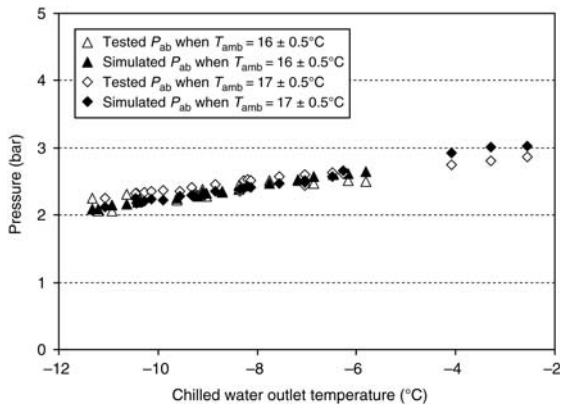

Figure 8. *Comparison between simulated and experimental pressures in the low pressure side of the system.*

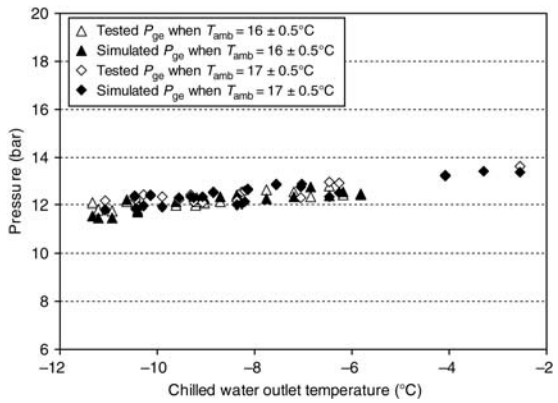

Figure 7. *Comparison between experimental and simulation results for the high pressure side of the system.*

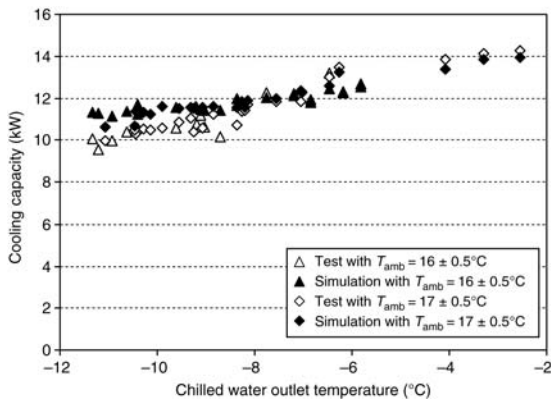

Figure 9. *Comparison between experimental and simulation results for cooling capacity.*

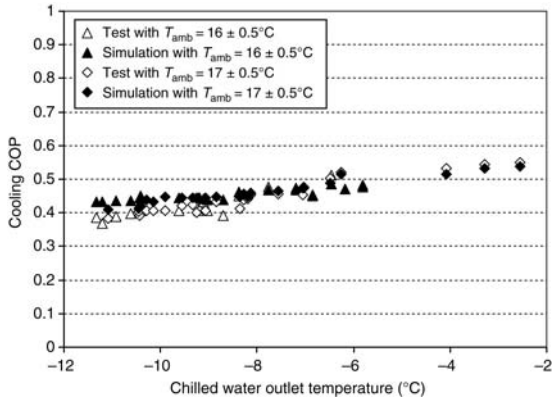

Figure 10. *Comparison between test and simulation results for coefficient of performance.*

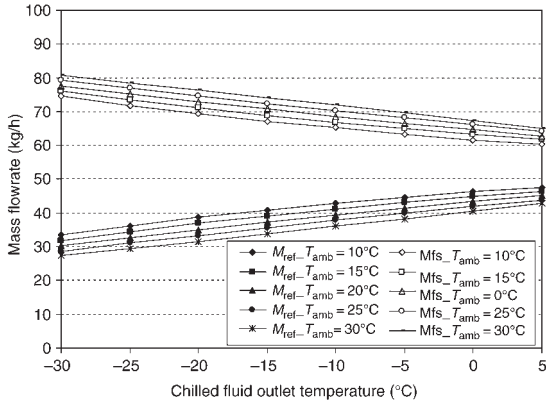

Figure 13. *Influence of chilled fluid flow temperature and ambient temperature on refrigerant and strong solution flow rates.*

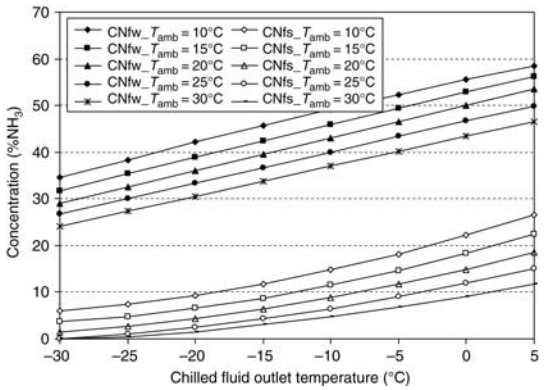

Figure 11. *Variation of ammonia concentration in strong and weak solution with chilled fluid and ambient temperature.*

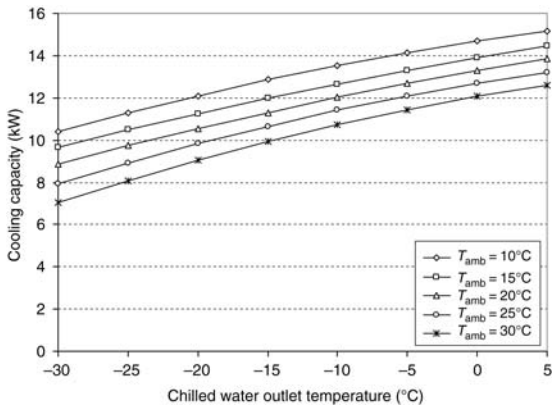

Figure 14. *Influence of chilled fluid flow temperature and ambient temperature on cooling capacity.*

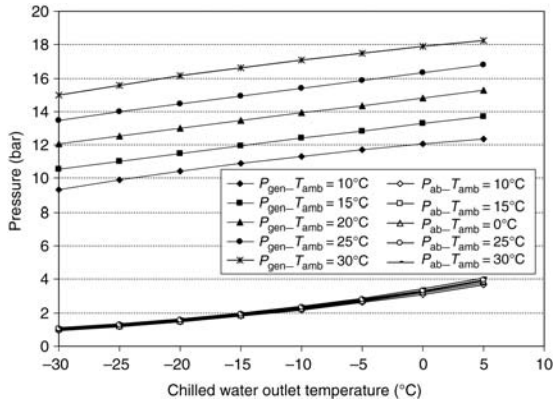

Figure 12. *Variation of pressure in the high and low pressure sides of the system with chilled fluid outlet temperature and ambient temperature.*

Figure 13 shows the variation of mass flow rate of refrigerant and strong solution with chilled fluid flow temperature and ambient temperature. It can be seen that as the chilled fluid and hence evaporating temperature increase, the refrigerant mass flow rate increases and as a consequence, the mass flow rate of the strong solution decreases. An increase in the ambient temperature, at constant generator heat input, causes a reduction in the refrigerant mass flow rate, because of its effect on condensing pressure and temperature and the refrigerant enthalpy entering the evaporator.

The increase of refrigerant flow rate with chilled fluid flow temperature leads to an increase in the cooling capacity as shown in Figure 14. It can also be seen that an increase in the ambient temperature causes a reduction in the cooling capacity because of its influence on the condensing pressure and temperature and the refrigerant enthalpy entering the evaporator. At constant energy input to the generator, the increase in the cooling capacity of the system leads to an increase in the COP as shown in Figure 15.

The chilled water outlet temperature of the chiller is controlled through the on–off control of the gas supply and heat input to the generator. To investigate the effect of heat input on the performance characteristics of the system, the model was run for a range of heat inputs and constant chilled fluid and air flow rates and temperatures at inlet to the evaporator and condenser, respectively. The results for a chilled fluid inlet temperature of 0°C, constant chilled water mass flow rate of

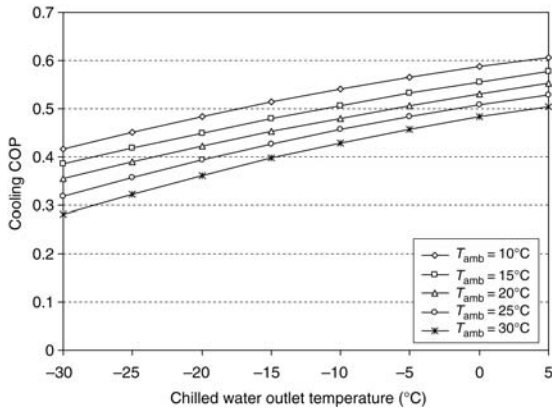

Figure 15. *Variation of cooling coefficient of performance with ambient and chilled fluid outlet temperature.*

Table 1. *Effect of variation of heat input to the generator on system performance*

Q_{gen} (kW)	P_g (bar)	P_a (bar)	$\dot{m}_r$ (kg/h)	ξ_s (%)	ξ_w (%)	Q_e (kW)	COP
20	11.25	2.87	36.07	25.69	50.54	11.26	0.56
22	11.89	2.78	38.71	21.51	49.62	12.15	0.55
24	12.45	2.69	41.32	17.03	48.74	12.96	0.54
26	12.94	2.62	43.90	12.26	47.89	13.68	0.53
28	13.36	2.56	46.44	7.19	47.07	14.31	0.51
30	13.70	2.51	48.94	1.82	46.28	14.85	0.49

COP, coefficient of performance.

0.7 kg/s, constant ambient temperature of 10°C and variation of heat input to the generator from 20 kW to 30 kW are shown in Table 1.

It can be seen that increasing the heat input to the generator will cause an increase in the generator pressure and a reduction in the absorber pressure. This is a result of the increase in the refrigerant flow rate in the system which will also result in a significant reduction in the concentration of refrigerant in the strong solution and a slight reduction in the concentration of refrigerant in the weak solution. The higher heat input and increased refrigerant flow rate will cause an increase in the cooling capacity of the system and a reduction in the chilled fluid flow temperature. The lower evaporating temperature and pressure will also lead to a reduction in the COP of the system.

5 CONCLUSIONS

A model of an ammonia–water absorption refrigeration system has been developed using the TRNSYS simulation environment. The model was validated against test results over a range of chilled fluid flow temperatures and ambient temperatures. These, together with the heat input to the generator are the main parameters that influence the performance of the system. Some meaningful results can be obtained from the simulation with the validated model, which can help to extensively understand the performance of the absorption system:

- The concentrations of both strong and weak solutions increase with higher chilled fluid outlet temperature at constant ambient air temperature but decrease with higher ambient air temperature at fixed chilled fluid outlet temperature. When ambient air temperature varies from 10°C to 30°C and the chilled fluid outlet temperature changes from −30°C to 5°C, the concentrations of strong and weak solutions fluctuate from 0.1% to 27.4% and from 22.4% to 58.9%, respectively.
- The ambient air temperature has little effect on pressures in the evaporator and absorber.
- At constant ambient air temperature, the higher chilled fluid outlet temperature leads to increased refrigerant mass flow rate but decreased strong solution mass flow rate. While at constant chilled fluid outlet temperature, the higher ambient temperature causes decreased refrigerant mass flow rate but increased strong solution mass flow rate. When ambient air temperature varies from 10°C to 30°C and the chilled fluid outlet temperature changes from −30°C to 5°C, the mass flow rates of refrigerant and strong solutions fluctuate from 26.3 kg/h to 47.8 kg/h and from 81.7 kg/h to 60.4 kg/h, respectively.
- The increase of generator heat input from 20 kW to 30 kW greatly decreases the concentration of strong solution (from 25.69% to 1.82%) but has little effect on the concentration of weak solution (from 50.54% to 46.28%) and eventually increases the cooling capacity from 11.26 kW to 14.85 kW but slightly decreases the COP from 0.56 to 0.49.

NOTATION

CHP	combined heat and power
COP	coefficient of performance
Dtsc	refrigerant subcooling of condenser outlet (K)
Dtsc	specified refrigerant subcooling of condenser outlet (K)
Dtsh	refrigerant superheating of evaporator outlet (K)
Dtshs	specified refrigerant superheating of evaporator outlet (K)
f	ratio of cycle
h	enthalpy (J/kg)
$\dot{m}$	mass flow rate (kg/s)
LMTD	logarithmic mean temperature difference (K)
M_{ref}	mass flow rate of refrigerant (kg/h)
M_{fs}	mass flow rate of strong solution (kg/h)
P_a	solution pressure inside absorber (bar)
P_g	solution pressure inside generator (bar)
Q	heat transfer rate (W)
q	heat transfer effect (J/kg)

R	ratio of return flow
T, t	temperature (°C, K)
T_{amb}	ambient air temperature (°C)
ΔT	temperature difference (K)
UA	overall conductance (W/K)
ξ	concentration (% by mass)

SUBSCRIPTS

*4*l	saturated liquid at point '4' in Figure 1
a	absorber, air
cf	chilled fluid
e	evaporator
g	generator
in	inlet
out	outlet
r	rectifier
s	strong solution (rich in absorbent)
p	pump
w	weak solution (weak in absorbent)

ACKNOWLEDGEMENTS

The authors wish to acknowledge the Food Technology Unit of DEFRA for their financial support for this project and the contribution of the industrial collaborators, Bond Retail Services Ltd, Apex Air Conditioning, Doug Marriott Associates and Bowman Power.

REFERENCES

[1] Faramarzi PT, Walker DH. Investigation of secondary loop supermarket refrigeration systems. *Consultant Report* 500-04-013, March 2004.

[2] Herold KE, Radermacher R, Klein S. *Absorption Chillers and Heat Pumps*. CRC Press, 1996.

[3] Lazzarin RM, Gasparella A, Longo GA. Ammonia-water absorption machines for refrigeration: theoretical and real performances. *Int. J. Refrigeration* 1996;**19**:239–46.

[4] Lazzarin RM, Gasparella A, Romagnoni P. Experimental report on the reliability of ammonia-water absorption chillers. *Int. J. Refrigeration* 1996;**19**:247–56.

[5] Horuz I, Callander TMS. Experimental investigation of a vapor absorption refrigeration system. *Int. J. Refrigeration* 2004;**27**:10–16.

[6] Grossman G, Perez-Blanco H. Conceptual design and performance analysis of absorption heat pumps for waste heat utilization. *Int. J. Refrigeration* 1982;**5**:361–70.

[7] Grossman G, Gommed K, Gadoth D. *A computer model for simulation of absorption systems in flexible and modular form of absorption systems in flexible and modular form (ORNL/Sub/90 = -89673)*. Oak Ridge National Laboratory, Oak Ridge, TN, 1991.

[8] Grossman G. Modular and flexible simulation of advanced absorption systems. In: *Proceedings of the International Absorption Heat Pump Conference*, Vol. **31**, AES, New Orleans, LA, 1994, 345–52.

[9] Grossman G, Wilk M. Advanced modular simulation of absorption systems. *Int. J. Refrigeration* 1994;**17**:231–44.

[10] Grossman G, Zaltash A. ABSIM-modular simulation of advanced absorption systems. *Int. J. Refrigeration* 2001;**24**:531–43.

[11] Chua HT, Toh HK, Malek A, Ng KC, Srinivasan K. A general thermodynamic framework for understanding the behaviour of absorption chillers. *Int. J. Refrigeration* 2000;**23**:491–507.

[12] Goel N, Goswami DY. Analysis of a counter-current vapour flow absorber. *Int. J. Heat Mass Transfer* 2005;**48**:1283–92.

[13] Kaynakli O, Horuz I. Comparison of parallel and counter flow coil absorber performance. *Int. J. Heat Mass Transfer* 2006;**33**:211–23.

[14] Kwon K, Jeong S. Effect of vapor flow on the falling-film heat and mass transfer of the ammonia/water absorber. *Int. J. Refrigeration* 2004;**27**:955–64.

[15] Conde M. Thermophysical properties of $\{NH_3 + H_2O\}$ solution for the industrial design of absorption refrigeration equipment. *M.Conde Engineering*, 2006.

[16] TRNSYS. *A Transient System Simulation program*. TRNSYS 16, 2005.